論文 / 著書情報
Article / Book Information

Title	Impact of Anthropogenic Heat on Air Temperature: A First-Order Estimate Using Dimensional Analysis and Numerical Simulations
Authors	Do Ngoc Khanh, Alvin C. G. Varquez, Manabu Kanda
Citation	Geophysical Research Letters, Vol. 52, Issue 11,
Pub. date	2025, 5
DOI	https://doi.org/10.1029/2024GL114400
Creative Commons	Information is in the article.

Geophysical Research Letters

RESEARCH LETTER
10.1029/2024GL114400

Special Collection:
Land-atmosphere coupling: measurement, modelling and analysis

Impact of Anthropogenic Heat on Air Temperature: A First-Order Estimate Using Dimensional Analysis and Numerical Simulations

Do Ngoc Khanh[1,2], **Alvin C. G. Varquez**[2], **and Manabu Kanda**[2]

[1]SIT Research Laboratories, Shibaura Institute of Technology, Tokyo, Japan, [2]Department of Transdisciplinary Science and Engineering, Institute of Science Tokyo, Tokyo, Japan

Key Points:

- A simple semi-theoretical semi-empirical relation was derived to predict temperature increase due to anthropogenic heat
- The temperature increase can be explained mainly by anthropogenic heat flux, planetary boundary layer height, wind speed, and city size

Supporting Information:

Supporting Information may be found in the online version of this article.

Correspondence to:

D. N. Khanh,
khanhdn@shibaura-it.ac.jp

Citation:

Khanh, D. N., Varquez, A. C. G., & Kanda, M. (2025). Impact of anthropogenic heat on air temperature: A first-order estimate using dimensional analysis and numerical simulations. *Geophysical Research Letters*, *52*, e2024GL114400. https://doi.org/10.1029/2024GL114400

Received 2 JAN 2025
Accepted 26 MAR 2025

Author Contributions:

Conceptualization: Do Ngoc Khanh
Formal analysis: Do Ngoc Khanh
Funding acquisition: Do Ngoc Khanh, Alvin C. G. Varquez, Manabu Kanda
Investigation: Do Ngoc Khanh
Methodology: Do Ngoc Khanh
Project administration: Manabu Kanda
Software: Do Ngoc Khanh
Validation: Alvin C. G. Varquez, Manabu Kanda
Visualization: Do Ngoc Khanh
Writing – original draft: Do Ngoc Khanh
Writing – review & editing: Do Ngoc Khanh, Alvin C. G. Varquez, Manabu Kanda

Abstract Anthropogenic heat is a strong point source in urban areas, increasing temperature and exacerbating heat-related health risks. While its impact on urban climate has been widely studied, a simple expression for quickly estimating temperature changes due to anthropogenic heat remains lacking. In this study, we derive such a relation by a novel integration of dimensional analysis with numerical simulations. Our findings show that under mean conditions, anthropogenic heat behaves similarly to a passive scalar, making planetary boundary layer height, wind speed, and urban surface area effective proxies for estimating additional warming. Incorporating radiation, a key factor distinguishing anthropogenic heat from a passive scalar, improves the physical consistency of the relation, particularly at low wind speeds.

Plain Language Summary Human activities (e.g., metabolism, air conditioning, traffic, and industry) release extra heat into the environment. This excess heat raises temperatures in cities and increases heat stress on people. In this study, we develop a simple equation to quickly estimate how much urban temperatures rise due to these heat emissions. Our findings show that this warming can be predicted using three key factors: the height of the atmosphere directly influenced by the surface (known as the planetary boundary layer height), city size, and wind speed, similar to how air pollution, like dust concentration, can be modeled. However, unlike pollutants, heat dispersion is also affected by radiation, which plays a crucial role at low wind speeds.

1. Introduction

Anthropogenic heat (AH) is heat generated by human activities (e.g., human metabolism, air conditioners, vehicles, and industry). The global average of AH over land was 0.10 W/m^2 in 2013 and is projected to increase to 2 to 3 times the 2013 level by the year 2100 due to growing economy, population, and energy consumption (Lu et al., 2017). Even though the global average of AH is small, because human settlements occupy only a small fraction (3%) of global land area (Schneider et al., 2009; Y. Zhou et al., 2015), AH is a strong point source.

From the energy balance perspective, AH can be treated as a source term aside from natural radiation terms (Oke et al., 2017). In general, the addition of AH will increase local temperature. Previous studies for many cities around the world have pointed out that AH caused a maximum of 0.15–3 K increase in air temperature in many cities around the world (see the review of L. Wang et al. (2023)). For example, AH may contribute up to half of the future total urban warming in Hanoi, a rapidly developing city in Vietnam (Doan et al., 2019). Beyond pure temperature change, feedbacks such as increases in precipitation (Kim et al., 2021; Nie et al., 2017) and various health risks (Lin et al., 2022; Zeng et al., 2022) were found to arise.

Focusing on the temperature aspect, while some observation campaigns have been conducted (Kikegawa et al., 2014), attributions of temperature increase to AH are usually done by simulation using numerical models because they allow more flexible experiment setups. However, numerical weather and computational fluid dynamics simulations are in general expensive. For practical purposes where a rough prediction (rather than a detailed spatiotemporal AH effect map) is sufficient, a quick first-order estimation of warming due to anthropogenic heat is desirable. However, such an expression has yet to be proposed. In this study, by applying dimensional analysis methods, we propose a relation that can serve as a first-order estimate of the AH impact.

2. Methods

We conducted simulations for 43 megacities (UN DESA, 2018) using the Weather Research and Forecast (WRF) model v4.6, which can model spatially varying urban morphological parameters, following the work by Khanh et al. (2023a). Using the AH4GUC present (2010s) and future (2050s) global hourly monthly 1 km resolution anthropogenic heat data set (Varquez et al., 2021), we prepared three scenarios: AH0 (inputting no AH), AH2010 (inputting the 2010s AH map), and AH2050 (inputting the 2050s AH map). The meteorological condition for all three scenarios is fixed to the 2006–2015 period (hereinafter, the 2010s) mean condition to isolate the AH effect. For each city and each scenario, simulations were conducted to obtain 12 days of data, with each day representing the ensemble average of a month of the year in the 2010s. Specifically, for example, for January, the ensemble average of the NCEP FNL 6-hourly reanalysis data set was taken for all days in the 2010s. That averaged condition is then repeatedly inputted to the WRF model to drive a 2-day simulation, one day for spin-up and one day for analysis. The latter one day can be considered a typical day in January in the 2010s because the input is the ensemble average of 10 years of reanalysis data. This method has been verified against ensemble averaged observation data sourced from the NOAA ISD database (see Table A1 of Khanh et al. (2023a)). Each simulation was conducted using one-way nesting with 6 and 2 km resolution domains (Figure S4 in Supporting Information S1). AH was emitted to the first modeled atmospheric level (Khanh et al., 2023a).

The AH2010 and AH2050 scenarios were compared against the AH0 scenario for analyzing the sensitivity of 2 m air temperature to AH. In this study, we only use the spatiotemporal average of all variables to focus on the bulk link between AH, air temperature, and other factors. Thus, there are 1,032 data points in total (43 cities × 12 months × 2 scenarios). In addition, urban grids are defined to be grids with a population density of at least 1,000 per square kilometer and an annual average AH of at least 1 W/m^2.

Although AH interacts actively with the atmosphere, here, we attempt to model the AH impact on air temperature (hereinafter, AH impact) as passive scalar concentration and assess the similarity between AH and passive scalars. Variables that can characterize this system are.

1. Q $\left(\mathrm{W}/\mathrm{m}^2\right)$: The inputted local anthropogenic heat flux.
2. ΔT (K): The change in near-surface air temperature due to the anthropogenic heat flux Q.
3. $\rho c_p \approx 1200\ \mathrm{J}/\mathrm{m}^3\ \mathrm{K}$: The volumetric heat capacity of air.
4. H (m): Planetary boundary layer (PBL) height (PBLH), the height to which the atmosphere is directly affected by the surface, an integrated outcome of surface properties, radiation, wind, atmospheric stability, and other factors. PBL contains almost all surface-atmosphere interactions (e.g., momentum, heat, and scalar concentration exchange). Therefore, PBLH may correlate to the upper extent to which AH impact can spread.
5. U (m/s): Wind speed. It is known that stronger wind can remove excess heat and pollutants from urban areas.
6. A $\left(\mathrm{m}^2\right)$: City area. In a larger city, it may take more time for AH to be advected out of the urban area boundary.

3. Results and Discussions

3.1. Sensitivity of Air Temperature to Anthropogenic Heat

Focusing on the six variables $Q, \Delta T, \rho c_p, H, U$, and A, because there are four dimensions (time, length, mass, and temperature), the following two dimensionless groups can be obtained by applying the Buckingham π theorem.

$$\pi_1 = \frac{H}{\sqrt{A}}, \quad \pi_2 = \frac{Q}{\rho c_p U \Delta T}. \tag{1}$$

We attempt to interpret the physical meaning of these dimensionless quantities by analyzing an ideal setup. Consider a square rectangular prism-shaped control volume (CV) with a height H, and a base side D (hence, a base area $A = D^2$), with closed bottom and top boundaries, open horizontal boundaries, and oriented parallel to the axes. A constant heat flux Q is released uniformly from the bottom surface while wind flows uniformly at speed U from west to east (see Figure S1 in Supporting Information S1 for a schematic sketch). For simplicity, variables representing thermal diffusion and radiation are not included yet. The key assumption for this model is perfect vertical mixing in the atmosphere within the PBL (i.e., temperature's vertical gradient is zero). Temperature is also uniform in the spanwise y-direction because of the west-east flowing wind. This setting ultimately transforms the problem into a one-dimensional problem along the streamwise x-direction.

We follow the Lagrangian approach of tracking each individual air parcel to determine its temperature. While not discussed in this study, the Lagrangian approach can also discuss contributions of individual heat sources to urban mean temperature by tracing the movement of each air parcel after leaving its original position. The change with time of AH impact ΔT on an air parcel can be described by the following ordinary differential equation (ODE),

$$\frac{\mathrm{d}\Delta T}{\mathrm{d}t} = \frac{Q}{H\rho c_p}. \tag{2}$$

Q spreads evenly within the PBL because of the perfect vertical mixing assumption. Given $\Delta T(0) = 0$, the solution to Equation 2 is

$$\Delta T(t) = \int_0^t \frac{Q}{H\rho c_p}\mathrm{d}t' = \frac{Qt}{H\rho c_p}, \tag{3}$$

which gives the AH impact on the air parcel at time t.

Next, we calculate the average temperature change of the CV $\overline{\Delta T}$ at the steady state. Observing that the temperature at a distance x ($0 \le x \le D$) from the west edge of the CV is $\Delta T(x/U)$ because the air parcel at position x is the one which spent a duration x/U to move from the west edge to arrive there. Thus, $\overline{\Delta T}$ can be obtained by averaging $\Delta T(x/U)$ across the CV using the following integral,

$$\overline{\Delta T} = \frac{1}{D}\int_0^D \Delta T(x/U)\mathrm{d}x = \frac{1}{\tau_c}\int_0^{\tau_c} \Delta T(t)\mathrm{d}t \tag{4}$$

where $\tau_c = D/U = \sqrt{A}/U\ (s)$. We refer to τ_c as the characteristic timescale of the system similar to its usage in the context of passive scalars (e.g., pollutants) dispersion to relate with scalar residence time (Duan et al., 2023; Lau et al., 2020). Physically, this quantity describes the time it takes for a passive scalar to be advected from the entry to the exit of the CV.

Calculating the integral in Equation 4 gives

$$\overline{\Delta T} = \frac{1}{\tau_c}\int_0^{\tau_c} \frac{Qt}{H\rho c_p}\mathrm{d}t = \frac{Q\tau_c}{2H\rho c_p} = \frac{Q\gamma}{2} = \frac{1}{2}\times\frac{Q}{\rho c_p U}\times\frac{\sqrt{A}}{H}, \tag{5}$$

where $\gamma = \tau_c/(H\rho c_p)$ for later usage. See Text S1 in Supporting Information S1 for derivations of Equations 4 and 5. Note that while the mathematical formulation is universal and can be applied to other CV shapes, without the symmetry of the square, the derivation of $\overline{\Delta T}$ will be more complex and may require numerical analysis.

Comparing with Equation 1, we can infer that

$$a = \pi_1/\pi_2 = 1/2, \tag{6}$$

and interpret that π_2 describes the relationship between heat flux, wind speed, and temperature change for a cubical CV; π_1 is a correction factor accounting for the deviation of the CV from the cubical shape.

We verify the applicability of this model in estimating the AH impact by inputting the simulated values into the following model and obtaining the parameters with Bayesian inference using the PyMC library (Abril-Pla et al., 2023).

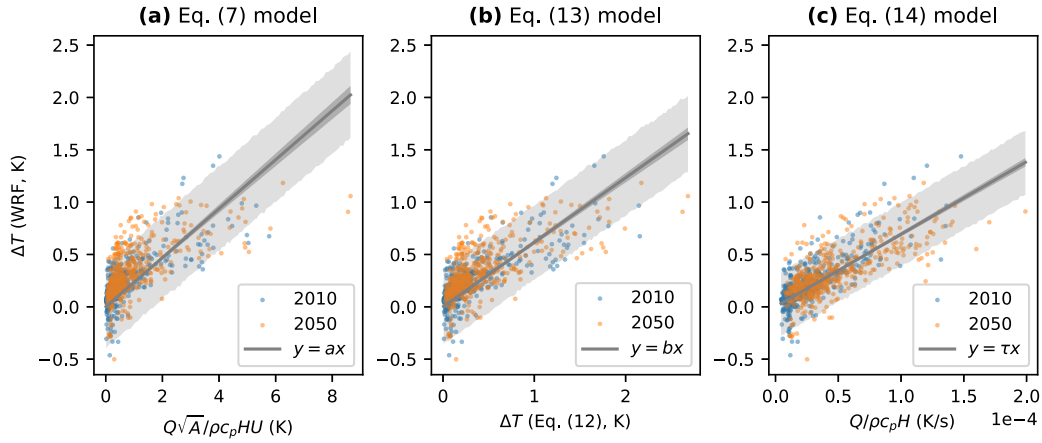

Figure 1. Comparison of three AH impact on temperature estimation models: (a) Passive scalar control volume model, $a = 0.234$ (dimensionless, Equation 7), (b) passive scalar control volume model with radiative feedback, $b = 0.616$ (dimensionless, Equation 13), and (c) residence time model, $\tau = 6930$ s (Equation 14). In all subfigures, the darker (very thin) shaded area represents the 95% credible interval (CI) of μ, which is the mean of the distribution of ΔT given a certain explanatory variables combination. The lighter (thicker) shaded area represents the 95% CI of ΔT. Blue (orange) dots are 516 data points from the AH2010 (AH2050) scenario.

$$\begin{aligned} \Delta T_i &\sim \text{Normal}(\mu_i, \sigma), \\ \mu_i &= a \times \frac{Q_i \sqrt{A_i}}{\rho c_p H_i U_i}, \\ a &\sim \text{Normal}(0.5, 0.25), \\ \sigma &\sim \text{HalfCauchy}(0, 1), \end{aligned} \tag{7}$$

where i is the index of each data point. As explained above, there are 1,032 data points. For each data point, ΔT is the mean difference of air temperature between the AH2010 and AH0 scenarios for the 2010s, and that between the AH2050 and AH0 scenarios for the 2050s. Q is from the AH4GUC data set. A is obtained by summing up the areas of urban grids. H and U are the harmonic means of PBLH and wind speed, respectively. Differences between the values of H and U before and after inputting AH are small (Figure S7 in Supporting Information S1). Because actual wind speed is not vertically constant as in the ideal setup, the vertical mean wind speed within the PBL is used to bridge this gap. Assuming that the power law holds, U can be estimated as

$$U = \frac{U_{10}}{\alpha + 1} \times \left(\frac{H}{10\ \text{m}} \right)^{\alpha}, \tag{8}$$

where $\alpha = 0.143$ (Text S4 in Supporting Information S1). The prior for a reflects the prior knowledge of its value derived from the ideal setup discussed above. The prior for σ is weakly informative. Note that the number of data points is large enough to overwhelm any reasonable prior; that is, the choice is not significantly influential.

As shown in Figure 1a, we found that $a = 0.234$ (dimensionless; highest density 95% credible interval (CI): 0.224–0.244) and $\sigma = 0.20$ K (95% CI: 0.195–0.213 K). The narrow CIs suggest that there is little uncertainty in the estimation of the mean effect as well as there is little uncertainty that the deviation from the mean effect is around 0.20 K. The model has a coefficient of determination R^2 of 0.40, a mean absolute error (MAE) of 0.15 K, and a root mean squared error (RMSE) of 0.20 K. The parameter σ implies that the deviation of simulated ΔT from the estimated mean effect μ by the model has a standard deviation $\sigma \approx 0.2$ K. This deviation will be discussed later in Section 3.3. The empirical coefficient a is equal to 46% of the ideal value of 0.5 derived in Equations 5 and 6 suggesting that the ideal model overestimates the AH impact, possibly due to omissions of mechanism or higher order terms that dampen the effect of AH. In the next section, we will explore one possible damping mechanism. Nevertheless, the similarity between the theoretical and empirical values of a suggests that the model is reasonable and the effect of AH on air temperature is not strongly nonlinear. Separate Bayesian

inferences were conducted for the 2010s and the 2050s and the derived parameters were the same (see Figure S2 in Supporting Information S1), hinting at the robustness of the model formulation.

Interpreting Equation 7, the following can be said about the AH impact on urban spatiotemporal mean air temperature.

1. The larger the city, the greater the AH impact because it takes a longer distance for hot air to exit city boundaries. Thus, the footprint of AH is more long-lasting. Previous research has also pointed out a potential link between urban heat island intensity (in which AH is a contributor) and city size (B. Zhou et al., 2017).
2. The higher the wind speed, the smaller the AH impact because hot air is advected out of the city faster. This is consistent with the choice of conducting AH observations on calm and fine days in past research (Kikegawa et al., 2014) and findings that AH impact and urban heat island intensity are stronger when wind is weak (He, 2018; Yuan et al., 2020; X. Wang et al., 2015).
3. The higher the PBLH, the smaller the AH impact because AH has more space to disperse vertically. This finding is also consistent with past research findings. For example, it is known that AH impact is stronger at nighttime than in daytime, and in winter than in summer because of the lower PBLH at nighttime and in winter compared to daytime and summer (Bohnenstengel et al., 2014; Khanh et al., 2023b; X. Wang et al., 2015). It is also consistent with the finding that the AH impact is strongly controlled by the exchange between the urban canopy and the upper atmosphere (L. Wang et al., 2023).

3.2. A Non-Passive Scalar Aspect of AH

Among three modes of heat transfer (conduction, convection, and radiation), convection has been considered in the previous section. Conduction is negligible in the atmosphere at city-scale because thermal diffusivity of air is 1.5×10^{-5} m^2/s at 0°C, resulting in a diffusion term several orders of magnitude smaller than the advection term at typical wind speed (order of 1 m/s). Thus, radiation is possibly one cause of the overestimation of ΔT by the ideal model in the previous section.

Specifically, the change in radiative heat flux emitted from the near-surface atmosphere when its temperature changes from T_a (before AH is applied) to $T_a + \Delta T$ (after AH is applied) can be expressed following the Stefan-Boltzmann law as

$$\Delta R = \varepsilon_a \sigma \left[(T_a + \Delta T)^4 - T_a^4 \right] \approx 4\varepsilon_a \sigma T_a^3 \Delta T = \beta \Delta T, \tag{9}$$

where ε_a is the emissivity of the atmosphere, σ is the Stefan-Boltzmann constant, and $\beta = 4\varepsilon_a \sigma T_a^3$ can be regarded as a damping coefficient against ΔT. While ε_a varies with atmospheric composition, we can take $\varepsilon_a = 0.8$ which is the value often used in the simple greenhouse effect model (Andrews, 2010, p. 7). The WRF model also captured a change in downward longwave heat flux consistent (in terms of trend and magnitude) with that predicted by the Stefan-Boltzmann law even though a lot of dispersion exists, reflecting the highly complex nature of atmospheric radiative processes (see Figure S5 in Supporting Information S1).

Now, we can modify the ODE in Equation 2 to include the radiative term as

$$\frac{\mathrm{d}\Delta T}{\mathrm{d}t} = \frac{Q - \beta \Delta T}{H \rho c_p}. \tag{10}$$

Similar to Equations 3 and 5, we can derive

$$\Delta T(t) = \frac{Q}{\beta}\left(1 - \exp\left(-\frac{\beta t}{H \rho c_p}\right)\right), \tag{11}$$

$$\overline{\Delta T} = \frac{1}{\tau_c}\int_0^{\tau_c} \Delta T(t)\mathrm{d}t = \frac{Q\gamma}{2} \times \frac{2[\beta\gamma - (1 - \exp(-\beta\gamma))]}{(\beta\gamma)^2} = \frac{Q\gamma}{2}\left(1 - \frac{\beta\gamma}{3}\right) + O\left((\beta\gamma)^2\right), \tag{12}$$

where $\gamma = \tau_c/(H\rho c_p) = \sqrt{A}/(H\rho c_p U)$, same as in Equation 5. See Text S2 in Supporting Information S1 for derivations of Equations 11 and 12. We observe that Equation 12 is Equation 5 multiplied by a damping factor

approximately $(1 - \beta\gamma/3)$. Without radiative feedback, γ is the only factor controlling the AH impact. With radiative feedback, γ is damped by β which is a function of T_a (air temperature when AH is zero). The damping factor is visualized in Figure S8 in Supporting Information S1.

We conduct another Bayesian inference to the fitness of the model with radiative feedback using weakly informative priors as follows.

$$\begin{aligned} \Delta T_i &\sim \text{Normal}(\mu_i, \sigma), \\ \mu_i &= b \times \overline{\Delta T}_{\text{Eq. (12)}}, \\ b &\sim \text{Normal}(0, 1), \\ \sigma &\sim \text{HalfCauchy}(0, 1), \end{aligned} \tag{13}$$

Note that b functions differently from a in Equation 7. a is a factor linking $\Delta T, Q, H, U$, and A, while b describes the similarity between the estimated mean effect by Equation 12 and the simulated ΔT by WRF. If the same model was fitted for Equation 5, we would get $b = a_{\text{empirical}}/a_{\text{theoretical}} = 0.234/0.5 = 0.468$.

We found that $b = 0.616$ (95% CI: 0.593–0.638) and $\sigma = 0.18$ K (95% CI: 0.18–0.19 K) (Figure 1b). The deviation σ will be discussed later in Section 3.3. In comparison with Equation 5, the prediction performance of Equation 14 is slightly higher ($R^2 = 0.48$, MAE = 0.13 K, and RMSE = 0.18 K). Overestimation was reduced by introducing the radiative feedback term (b increased from 0.468 to 0.616, which is closer to one). Nevertheless, overestimation still remains after first-order terms (i.e., mean terms) of conduction, convection, and radiation are all considered. This finding suggests that some higher order terms are damping AH effect and omitting them forces adjustment of first-order terms by a factor smaller than one. Future studies may try identifying these terms and their contributions.

Equation 12 is a damped version of Equation 5, thus, can be interpreted similarly. However, a critical difference that arises from the radiative feedback is the behavior of the estimated $\overline{\Delta T}$ in no wind condition (i.e., $U \to 0$ implying $\gamma \to \infty$). Equation 5 predicts that $\overline{\Delta T}$ unrealistically diverges to infinity as $U \to 0$ because AH is not advected away. On the contrary, Equation 12 predicts that $\overline{\Delta T}$ converges to $Q/\beta = Q/\left(4\varepsilon_a \sigma T_a^3\right)$ (derived in Text S3 in Supporting Information S1). While mean wind speed over the 3D-space of cities is rarely zero, this analysis confirms that the model with radiative feedback is more physical than the one without. It also highlights a crucial difference between passive scalars and AH. Specifically, while passive scalars can accumulate to extreme concentrations, air heated by AH will radiate back some energy (to be absorbed by other materials with higher heat capacity or to space) until a new equilibrium is reached.

3.3. The Residence Time of AH

We started in Section 3.1 with a dimensional analysis, and moved on to Section 3.2 with a more theoretical discussion. In this session, we attempt to go more statistical and less theoretical. Mimicking the residence time concept of passive scalars, we attempt to find a relation between $\overline{\Delta T}, Q, H$ and τ_c, which can be interpreted as a timescale describing how long AH resides in cities before being dissipated away, implicitly encompassing effects of A, U and radiative feedback. Equation 7 is then transformed to form a new statistical model as follows.

$$\begin{aligned} \Delta T_i &\sim \text{Normal}(\mu_i, \sigma), \\ \mu_i &= \tau \times \frac{Q_i}{\rho c_p H_i}, \\ \tau &\sim \text{Normal}(0.5, 2) \times 10^4, \\ \sigma &\sim \text{HalfCauchy}(0, 1), \end{aligned} \tag{14}$$

where the prior for τ and σ are weakly informative. We verified this relation by comparing $Q/\rho c_p H$ with ΔT in Figure 1c. By Bayesian inference, we found that $\tau = 6930$ s ≈ 2 h (95% CI: 6,730–7,130 s) and $\sigma = 0.16$ K (95% CI: 0.15–0.16 K). Among three models, the prediction performance of this model is the highest ($R^2 = 0.54$, MAE = 0.12 K, and RMSE = 0.16 K). Note that we also used the harmonic temporal mean for H similar to the

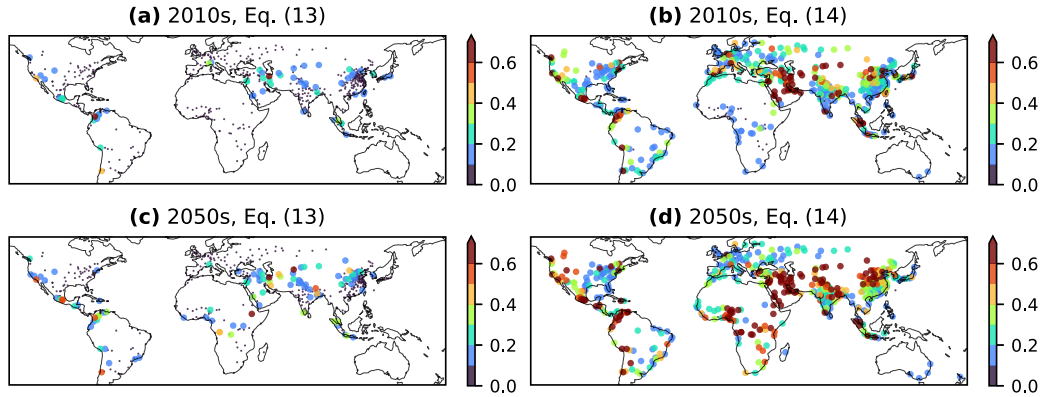

Figure 2. A first-order estimate of AH impact on temperature (K) for 626 cities with populations of at least one million by applying (a) Equation 13 in the 2010s, (b) Equation 14 in the 2010s, (c) Equation 13 in the 2050s, and (d) Equation 14 in the 2050s. Cities with AH impact of less than 0.1 K are plotted using tiny dots due to their large number. See Table S1 for tabulated data.

regression of Equation 7. It can then be interpreted that, as a first-order estimate, AH resides in cities for roughly 2 hr after being emitted before being removed from the megacities. This value suggests that regionally, AH effects are rather short-lived. This is possibly one reason why the AH impact is linear and resembles a passive scalar. However, it should be noted that AH still remains in the Earth system after removal from cities. Thus, AH may continue making some, possibly long-lived, impacts beyond the urban boundaries. For comparison, residence time of airborne pollutants in avenue and streets in Hong Kong (local scale) is in the order of hundreds of seconds (Lau et al., 2020), pollutants residence times in four UK cities (city scale) are likely to be a few hours (Harrison, 2018), while air parcel residence times in the Pearl River Delta, China (regional scale) are roughly 10–20 hr (Huang et al., 2019).

We now discuss the standard deviation σ from the mean effect μ. The mean values for the three models in Equations 7, 13 and 14 are 0.20, 0.18, and 0.16 K, respectively. Monthly residuals are shown in Figure S6 in Supporting Information S1. All deviations are close to each other despite the inclusion and exclusion of radiative feedback, city area, and wind speed, as well as the theoretical or statistical nature of the model. This suggests that the deviation σ is not significantly influenced by these factors. We hypothesized that these variability are likely caused by missing factors such as geographical features (e.g., topography) and physical processes (e.g., moisture). The source of variability can be further investigated by adding factors one by one to the theory or removing factors one by one from the WRF simulation. However, this task is beyond this study's scope.

3.4. Applicability and Limitations of the First-Order Estimate

To demonstrate the applicability of the derived relations, we estimated the historical and potential future AH impact for 626 urban agglomerations (hereinafter, cities) with populations of at least one million indexed by the City Population database (Brinkhoff, 2024) using two models: Equation 13 (semi-theoretical with radiative feedback) and Equation 14 (statistical). Input variables are AH (the AH4GUC 2010s and 2050s AH data set), meteorological variables (wind speed and PBLH) extracted from the ERA5 reanalysis data set (2006–2015 period), and city size estimated from the MCD12Q1.061 MODIS Land Cover 2022 data set. All datasets were upscaled to the 0.25° resolution of ERA5. We calculated the monthly mean of AH and the decade monthly mean of meteorological variables and input them to Equation 7 to get 12 values representing the mean effects in 12 months of a year. Then, we averaged the 12 values to obtain the annual mean in the 2010s and the 2050s shown in Figures 2a and 2c, respectively. The same procedure was applied for another estimation using Equation 14 (Figures 2b and 2d). The full data set for all 626 cities is provided in Table S1 in CSV format. To isolate AH impacts, we assume that meteorological variables and city size do not change between the 2010s and the 2050s. Combined impacts of AH, urbanization, and climate change can be considered in another study in the integrated assessment context.

The semi-theoretical model (Equation 13) predicts that for 567 of 626 cities, the contribution of AH to air temperature in the 2010s (Figure 2a) is weak (less than 0.1 K) as a first-order estimate. Comparison between

$\Delta T/Q$ estimated here and the values in the literature (L. Wang et al., 2023) shows that the values are largely consistent despite various differences in methodology and spatiotemporal focus (Figure S10 in Supporting Information S1). AH contribution exceeds 0.1 and 0.2 K in only 59 cities (9.4%) and 23 cities (3.7%), respectively. Cities with strong AH impacts are characterized by low PBLH and weak wind (Medellín (Colombia): 0.65 K, Santiago (Chile): 0.45 K, and Turin (Italy): 0.33 K), high AH flux and low PBLH (Tehran (Iran): 0.90 K), high AH flux and large city area (Los Angeles (US): 0.41 K, Seoul (South Korea): 0.22 K). Note that the discussed properties of cities (e.g., weak wind, low PBLH) are relative in comparison with the other cities. In the 2050s (Figure 2c), the number of cities with AH impacts larger than 0.1 K increases to 106 (16.9%), nearly doubling the 2010s figure. Newly affected cities are in the US, Central Africa, Eastern China, and along the Himalayas. This difference between the 2010s and the 2050s is certainly due to the increase in AH flux because, as an assumption for this analysis, all other variables are kept constant to isolate the AH effects. However, as also discussed above, some cities have meteorological conditions allowing more visible AH impact on temperature. For example, cities located near the Himalayas are more prone to AH impact because they have low PBLH (captured by ERA5 and confirmed in previous observations (Slättberg et al., 2022)). This analysis shows that the AH impact is not always attributable to any individual factor but results from the interaction between artificial causes (AH flux, city area) and natural causes (PBLH, wind speed). Smaller cities with lower AH flux can experience strong effects due to low PBLH (e.g., Medellín (Colombia): 0.65 K impact for 25.9 W/m^2 AH flux) while larger cities with high AH flux can experience small effects thanks to strong wind and high PBLH (e.g., Hong Kong (China): 0.11 K impact for 86.5 W/m^2 AH flux). In addition, because the standard deviation of the ΔT distribution (Equation 13) is $\sigma \approx 0.2$ K, a small mean does not imply a small effect at all times.

On the other hand, the pure empirical model (Equation 14) gives a distinct estimate that, in the 2010s, 520 cities (83.1%) and 182 cities (29.1%) experienced AH impact exceeding 0.1 and 0.3 K, respectively (Figure 2b). In the 2050s, these numbers rise to 589 (94.1%) and 303 (48.4%), respectively (Figure 2d). With only two explanatory variables (AH and PBLH), interpreting this model is simple. Specifically, the model suggests that the AH impact is higher in cities with higher AH flux and lower PBLH (Figure S3 in Supporting Information S1). Because of the 2 hour residence time assumption, it can be interpreted that given some meteorological conditions delaying AH dissipation to 2 hours (e.g., weak wind, stable atmospheric stratification), AH impact on temperature can be strong. Thus, this estimation may be a warning sign for many cities and further research on the AH impact focusing on various types of local meteorological events is recommended. However, as an estimation of the (annual) mean AH impact, this pessimistic estimation should be interpreted with caution because the 2 hour AH residence time assumption in Equation 14 ignores wind speed and city size considered in Equation 13. Because Equation 13 is a modified version of Equation 7, we can compare the simpler Equation 7 with Equation 14 to identify the essential difference between the two AH impact predictions. Dividing Equation 7 by Equation 14, we have $\Delta T_{\text{Eq. (7)}}/\Delta T_{\text{Eq. (14)}} = (\alpha/\tau) \times (\sqrt{A}/U)$. The ratio $\Delta T_{\text{Eq. (13)}}/\Delta T_{\text{Eq. (14)}}$ should be essentially the same (confirmed by Figure S9 in Supporting Information S1). In other words, Equation 13's prediction is smaller than Equation 14's prediction because most cities have small $\sqrt{A}/U$.

Therefore, the two predictions are not contradictory: the semi-theoretical Equation 13 predicts the annual mean AH impact, while the pure empirical Equation 14 predicts the AH impact on a hypothetical 2 hour AH residence time event. We note that results with large differences between models are not unrecorded. It was previously pointed out that in dynamical atmospheric modeling, just by minor changes in model structure, the estimated AH impact on canopy air temperature can vary by an order of magnitude (Li et al., 2024). That is to say, regardless of physical, semi-theoretical, or statistical modeling, uncertainties in the AH impact are expected. Thus, further investigation into these kinds of uncertainties is recommended.

The example above shows that the proposed semi-empirical relation can provide a quick look at the historical and potential future AH contributions to urban warming. However, the treatment of AH as a passive scalar imposes some limits on the relation's applicability. For example, the AH flux should be small enough not to significantly change the PBLH or wind circulation imposed by the background forcing. Despite that limit, the passive scalar treatment may allow the relation to also predict concentrations of pollutants.

4. Concluding Remarks

In this study, by combining dimensional analysis techniques, Lagrangian air parcel tracking idealized model, and numerical weather simulation, we proposed a simple relationship linking temperature change due to

anthropogenic heat (AH) to boundary layer height, wind speed, and urban surface area. The relation can be used as a first-order estimate of the impact of AH on near-surface air temperature without the need for running additional numerical simulations. The relation was verified to have decent prediction performance. A radiative feedback term was introduced to the idealized model to reduce overestimation and improve physical consistency in low wind speed cases. We also proposed the concept of residence time of AH. We found that the immediate AH impact on urban temperature has a short time span of about 2 hours. However, this finding does not exclude the possibility of some long-term impacts of AH on cities and the overall atmospheric system. We recommend the usage of general circulation models (GCMs) to investigate the long-term impacts of AH on the global atmospheric system in future studies. Further research on physical processes affecting the residence time of AH is also recommended. While the data used in this study comes from 43 megacities, which are geographically and socio-economically diverse, future studies may conduct further sensitivity analysis by including smaller cities, perturbing wind fields, and perturbing some variables that can change the diagnostic PBLH.

Applying the relationship to 626 cities with populations of at least one million, we found that, as a first-order estimate, the mean AH impact on air temperature is generally less than 0.1 K for most cities even in the 2050s, but the standard deviation from the mean effect is about 0.2 K. The impact can be larger for cities with specific meteorological conditions such as low planetary boundary layer height or weak wind. This annual mean estimation has to be clearly distinguished from higher spatial or temporal peak values reported in other studies (Doan et al., 2019; Ma et al., 2017; Zhang et al., 2016). Given the right conditions which can delay AH dissipation to just 2 hr, the AH impact can be much larger (exceeding 0.3 K in 48.4% of cities (Figure 2, Table S1)). Thus, research focusing on AH impacts under various meteorological events is recommended. Moreover, a small spatiotemporal mean does not imply insignificance because the standard deviation of approximately 0.2 K was pointed out in this study and the finding that the impact of urbanization and anthropogenic heat on air temperature can have large spatial variance despite a small mean (Darmanto et al., 2019; Khanh et al., 2023a) has been pointed out in previous studies.

Data Availability Statement

The WRF model v4.6 is available at https://github.com/wrf-model/WRF/releases/tag/v4.6.0. The AH4GUC data set (Varquez et al., 2021) and the urban morphological parameters data set (Khanh et al., 2023a) are available from the corresponding references. Tabulated data for the 626 cities is provided in Table S1.

Acknowledgments
This study was supported by JSPS KAKENHI Grant JP21H04573, JP21K14249, and JP24K22982. The authors declare no conflicts of interest. The authors thank Prof. Tsuyoshi Kinouchi and the reviewers for their constructive comments and suggestions.

References

Abril-Pla, O., Andreani, V., Carroll, C., Dong, L., Fonnesbeck, C. J., Kochurov, M., et al. (2023). PyMC: A modern, and comprehensive probabilistic programming framework in Python. *Peer Journal Computer Science*, *9*, e1516. https://doi.org/10.7717/peerj-cs.1516

Andrews, D. G. (2010). *An introduction to atmospheric physics (2nd ed.)*. Cambridge University Press.

Bohnenstengel, S. I., Hamilton, I., Davies, M., & Belcher, S. E. (2014). Impact of anthropogenic heat emissions on London's temperatures. *Quarterly Journal of the Royal Meteorological Society*, *140*(679), 687–698. https://doi.org/10.1002/qj.2144

Brinkhoff, T. (2024). City population. Retrieved from https://www.citypopulation.de/

Darmanto, N. S., Varquez, A. C. G., Kawano, N., & Kanda, M. (2019). Future urban climate projection in a tropical megacity based on global climate change and local urbanization scenarios. *Urban Climate*, *29*, 100482. https://doi.org/10.1016/j.uclim.2019.100482

Doan, Q.-V., Kusaka, H., & Nguyen, T. M. (2019). Roles of past, present, and future land use and anthropogenic heat release changes on urban heat island effects in Hanoi, Vietnam: Numerical experiments with a regional climate model. *Sustainable Cities and Society*, *47*, 101479. https://doi.org/10.1016/j.scs.2019.101479

Duan, G., Nakamae, K., & Takemi, T. (2023). Impacts of urban morphometric indices on ventilation. *Building and Environment*, *229*, 109907. https://doi.org/10.1016/j.buildenv.2022.109907

Harrison, R. M. (2018). Urban atmospheric chemistry: A very special case for study. *npj Climate Atmospheric Science*, *1*(1), 20175. https://doi.org/10.1038/s41612-017-0010-8

He, B.-J. (2018). Potentials of meteorological characteristics and synoptic conditions to mitigate urban heat island effects. *Urban Climate*, *24*, 26–33. https://doi.org/10.1016/j.uclim.2018.01.004

Huang, Y., Yao, T., Fung, J. C. H., Lu, X., & Lau, A. K. H. (2019). Application of air parcel residence time analysis for air pollution prevention and control policy in the Pearl River Delta region. *Science of the Total Environment*, *658*, 744–752. https://doi.org/10.1016/j.scitotenv.2018.12.205

Khanh, D. N., Varquez, A. C. G., & Kanda, M. (2023a). Impact of urbanization on exposure to extreme warming in megacities. *Heliyon*, *9*(4), e15511. https://doi.org/10.1016/j.heliyon.2023.e15511

Khanh, D. N., Varquez, A. C. G., & Kanda, M. (2023b). Multi-megacity investigation of heat wave events under various climate change and urbanization scenarios. *Journal of JSCE*, *12*(2), 23–16120. https://doi.org/10.2208/journalofjsce.23-16120

Kikegawa, Y., Tanaka, A., Ohashi, Y., Ihara, T., & Shigeta, Y. (2014). Observed and simulated sensitivities of summertime urban surface air temperatures to anthropogenic heat in downtown areas of two Japanese major cities, Tokyo and Osaka. *Theoretical and Applied Climatology*, *117*(1–2), 175–193. https://doi.org/10.1007/s00704-013-0996-8

Kim, G., Cha, D.-H., Song, C.-K., & Kim, H. (2021). Impacts of anthropogenic heat and building height on urban precipitation over the Seoul metropolitan area in regional climate modeling. *Journal of Geophysical Research: Atmospheres*, *126*(23), e2021JD035348. https://doi.org/10.1029/2021JD035348

Lau, G. E., Ngan, K., & Hon, K. K. (2020). Residence times of airborne pollutants in the urban environment. *Urban Climate*, *34*, 100711. https://doi.org/10.1016/j.uclim.2020.100711

Li, D., Sun, T., Yang, J., Zhang, N., Vahmani, P., & Jones, A. (2024). Structural uncertainty in the sensitivity of urban temperatures to anthropogenic heat flux. *Journal of Advances in Modeling Earth Systems*, *16*(10), e2024MS004431. https://doi.org/10.1029/2024MS004431

Lin, L.-Z., Su, F., Fang, Q.-L., Ho, H. C., Zhou, Y., Ma, H.-M., et al. (2022). The association between anthropogenic heat and adult hypertension in Northeast China. *Science of the Total Environment*, *815*, 152926. https://doi.org/10.1016/j.scitotenv.2022.152926

Lu, Y., Wang, H., Wang, Q., Zhang, Y., Yu, Y., & Qian, Y. (2017). Global anthropogenic heat emissions from energy consumption, 1965–2100. *Climate Change*, *145*(3–4), 459–468. https://doi.org/10.1007/s10584-017-2092-z

Ma, S., Pitman, A., Hart, M., Evans, J. P., Haghdadi, N., & MacGill, I. (2017). The impact of an urban canopy and anthropogenic heat fluxes on Sydney's climate. *International Journal of Climatology*, *37*(S1), 255–270. https://doi.org/10.1002/joc.5001

Nie, W., Zaitchik, B. F., Ni, G., & Sun, T. (2017). Impacts of anthropogenic heat on summertime rainfall in Beijing. *Journal of Hydrometeorology*, *18*(3), 693–712. https://doi.org/10.1175/JHM-D-16-0173.1

Oke, T. R., Mills, G., Christen, A., & Voogt, J. A. (2017). *Urban climates*. Cambridge University Press.

Schneider, A., Friedl, M. A., & Potere, D. (2009). A new map of global urban extent from MODIS satellite data. *Environmental Research Letters*, *4*(4), 044003. https://doi.org/10.1088/1748-9326/4/4/044003

Slättberg, N., Lai, H.-W., Chen, X., Ma, Y., & Chen, D. (2022). Spatial and temporal patterns of planetary boundary layer height during 1979–2018 over the Tibetan Plateau using ERA5. *International Journal of Climatology*, *42*(6), 3360–3377. https://doi.org/10.1002/joc.7420

UN DESA. (2018). *The world's cities in 2018–data booklet*. UN. https://doi.org/10.18356/c93f4dc6-en

Varquez, A. C. G., Kiyomoto, S., Khanh, D. N., & Kanda, M. (2021). Global 1-km present and future hourly anthropogenic heat flux. *Scientific Data*, *8*(1), 64. https://doi.org/10.1038/s41597-021-00850-w

Wang, L., Sun, T., Zhou, W., Liu, M., & Li, D. (2023). Deciphering the sensitivity of urban canopy air temperature to anthropogenic heat flux with a forcing-feedback framework. *Environmental Research Letters*, *18*(9), 094005. https://doi.org/10.1088/1748-9326/ace7e0

Wang, X., Sun, X., Tang, J., & Yang, X. (2015). Urbanization-induced regional warming in Yangtze River Delta: Potential role of anthropogenic heat release. *International Journal of Climatology*, *35*(15), 4417–4430. https://doi.org/10.1002/joc.4296

Yuan, C., Adelia, A. S., Mei, S., He, W., Li, X.-X., & Norford, L. (2020). Mitigating intensity of urban heat island by better understanding on urban morphology and anthropogenic heat dispersion. *Building and Environment*, *176*, 106876. https://doi.org/10.1016/j.buildenv.2020.106876

Zeng, P., Sun, F., Shi, D., Liu, Y., Zhang, R., Tian, T., & Che, Y. (2022). Integrating anthropogenic heat emissions and cooling accessibility to explore environmental justice in heat-related health risks in Shanghai, China. *Landscape and Urban Planning*, *226*, 104490. https://doi.org/10.1016/j.landurbplan.2022.104490

Zhang, N., Wang, X., Chen, Y., Dai, W., & Wang, X. (2016). Numerical simulations on influence of urban land cover expansion and anthropogenic heat release on urban meteorological environment in Pearl River Delta. *Theoretical and Applied Climatology*, *126*(3–4), 469–479. https://doi.org/10.1007/s00704-015-1601-0

Zhou, B., Rybski, D., & Kropp, J. P. (2017). The role of city size and urban form in the surface urban heat island. *Scientific Reports*, *7*(1), 4791. https://doi.org/10.1038/s41598-017-04242-2

Zhou, Y., Smith, S. J., Zhao, K., Imhoff, M., Thomson, A., Bond-Lamberty, B., et al. (2015). A global map of urban extent from nightlights. *Environmental Research Letters*, *10*(5), 054011. https://doi.org/10.1088/1748-9326/10/5/054011